

# Photoinduced charge shift in Li<sup>+</sup> doped giant nested fullerenes

*Anton J. Stasyuk,<sup>a\*</sup> Olga A. Stasyuk,<sup>a</sup> Miquel Solà<sup>a\*</sup> and Alexander A. Voityuk<sup>a,b\*</sup>*

a Institut de Química Computacional and Departament de Química, Universitat de Girona, C/  
Maria Aurèlia Capmany 69, 17003 Girona, Spain.

b Institució Catalana de Recerca i Estudis Avancats, 08010 Barcelona, Spain.

carbon nano-onion • electron transfer • fullerene • excited state

## ABSTRACT

Over the last years, carbon nano-onions (CNOs) have been in focus in material science research. Their red-shifted absorption allows utilizing CNOs as promising photosensitizers. We report here a systematic study of excited state properties of six double-layered Li<sup>+</sup> doped fullerenes of  $I_h$  symmetry: [Li@C<sub>60</sub>@C<sub>240</sub>]<sup>+</sup>, [Li@C<sub>60</sub>@C<sub>540</sub>]<sup>+</sup>, [Li@C<sub>60</sub>@C<sub>960</sub>]<sup>+</sup>, [Li@C<sub>240</sub>@C<sub>540</sub>]<sup>+</sup>, [Li@C<sub>240</sub>@C<sub>960</sub>]<sup>+</sup> and [Li@C<sub>540</sub>@C<sub>960</sub>]<sup>+</sup>. On the basis of TDDFT calculations, we show that the long-wave absorption by the Li<sup>+</sup> doped species leads to charge transfer (CT) between the inner and the outer shells unlike their neutral double-layered precursors. The CT energy depends strongly on the size of the concentric fullerenes and it can easily be tuned by varying both the encapsulated metal ion and the size of the shells. Two types of low-lying excited states are identified (1)

capacitor-like structures, as  $\text{Li}^+@C_{60}^-@C_{240}^+$ , with alternating positive and negative charges, and (2) states, where the positive charge is delocalized over the outer shell, as in  $\text{Li}@C_{240}@C_{540}^+$ . We suggest a simple expression to estimate the energy difference of these excited states and to predict the type of the lowest CT state in nested fullerenes. The effect of nature of the encapsulated ion on the charge transfer state energies is considered. The HOMO – LUMO transition energy is found to vary significantly when going from  $[\text{Li}@C_{60}@C_{240}]^+$  to  $[\text{Li}@C_{540}@C_{960}]^+$ .

## 1. INTRODUCTION

Multiwall fullerenes, also known as carbon nano-onions (CNOs), hyperfullerenes or onion-like fullerenes are spherical or polyhedral nanoparticles of pure carbon. They consist of several stacks of graphene-like shells; each of them forms a closed structure on a linear scale of 10 nm.<sup>1</sup> Discovered by Iijima<sup>2</sup> in 1980 in amorphous carbon black, CNOs were synthesized and described by Ugarte<sup>3</sup> only twelve years later. The first experimental observation of double- and triple-layered CNOs was reported by Mordkovich in 2000.<sup>4</sup> Nowadays, different large-scale preparation approaches, such as decomposition of the carbon-containing precursor in presence of a catalyst,<sup>5</sup> thermal annealing of detonation nanodiamond powders,<sup>6,7</sup> and others,<sup>8-11</sup> exist for the synthesis of CNOs. Functionalized analogs of CNOs with largely improved solubility are used as electrode materials for capacitors,<sup>12,13</sup> anode materials for Li-ion batteries,<sup>14,15</sup> terahertz-shielding devices,<sup>16,17</sup> and have numerous biological applications.<sup>18-21</sup> Applicability of CNOs functionalized with NIR-emitting aza-borondipyrromethenes<sup>22,23</sup> for high-resolution cellular imaging has also been reported. Additionally, it has been recently demonstrated that photoluminescence is observed in CNOs.<sup>24</sup> Since preparation, separation, and analysis of properties of double- and triple-layered CNOs of a predetermined composition and structure are still very challenging<sup>25</sup> and cumbersome,

computational modeling appears to be a quite attractive tool to predict ground and excited state properties of such systems. The relatively large size of CNOs, however, limits the use of high-level *ab initio* and DFT methods. Among several considered CNOs, the smallest double-layered nano-onion  $C_{60}@C_{240}$  is the most intensively studied model.<sup>26-29</sup> The stabilization energy of CNOs is determined essentially by the dispersion interactions between layers and changes remarkably with their size.<sup>26-28</sup> The interaction energy between the outer and the inner shells in  $C_{60}@C_{240}$  is -144.0 kcal/mol, whereas in  $C_{240}@C_{540}$  it is -489.6 kcal/mol at PBE0-D3/def2-TZVP level of theory.<sup>28</sup> The interactions between individual layers in triple-layered CNOs is found to be superadditive.<sup>27</sup> In particular, the stabilization energy in  $C_{60}@C_{240}@C_{540}$  is found to be by 25 kcal/mol larger than the sum of interactions in  $C_{60}@C_{240}$  and  $C_{240}@C_{540}$ .

Here, we report a systematic computational study of structural and electronic properties in a series of double-layered CNOs constructed from  $I_h$  symmetrical fullerenes following the isolated pentagon rule (IPR), namely,  $C_{60}@C_{240}$ ,  $C_{60}@C_{540}$ ,  $C_{60}@C_{960}$ ,  $C_{240}@C_{540}$ ,  $C_{240}@C_{960}$ , and  $C_{540}@C_{960}$ , and their  $Li^+$  doped derivatives. The latter systems are particularly interesting because lithium-ion doped fullerenes show long lifetimes for charge separated (CS) states.<sup>30,31</sup> Given that the CS states in  $Li^+$  doped CNOs are of the lowest energy, the main attention in this work is paid to analysis of electron transfer (ET) between the shells caused by light absorption. Two types of low-lying excited states are identified (1) capacitor-like structures, as  $Li^+@C_{60}^-@C_{240}^+$ , with alternating positive and negative charges, and (2) states where the positive charge is delocalized over the outer shell, as in  $Li@C_{240}@C_{540}^+$ . The excitation energy is found to decrease from 1.70 eV in  $[Li@C_{60}@C_{240}]^+$  to 0.04 eV in  $[Li@C_{540}@C_{960}]^+$  changing significantly the electrical properties of the systems.

## 2. COMPUTATIONAL DETAILS

### 2.1 *General Methods.*

Geometry optimization, electronic structures calculations and vertical excitation energies were calculated using Tamm-Dancoff approximation (TDA)<sup>32</sup> with the range-separated CAM-B3LYP functional of Handy and coworkers<sup>33</sup> using Gaussian 16 (rev. A03)<sup>34</sup> and Pople's 6-31G(d) basis set.<sup>35</sup> The empirical dispersion D3 correction with Becke–Johnson damping<sup>36,37</sup> was employed. TDA is a popular method in computational chemistry because it is formally simpler than the full Casida formalism by setting matrix **B** to zero (see Eqs. S3-S7, SI), thus saving computational time.<sup>38,39</sup> It is also worthwhile to note that for a long-range CT state in the time-dependent density functional theory (TDDFT) the **B** matrix vanishes, which is equivalent to applying the Tamm-Dancoff approximation. Thus, TDDFT and TDDFT/TDA yield identical results for the excitation energies of long-range CT states.<sup>39</sup> Another benefit of the TDA is that it allows avoiding singlet and triplet instabilities and thus is highly useful for calculations of excited-state potential energy surfaces.<sup>40,41</sup> It was also demonstrated that TDA is in a good agreement with both TDDFT and experimental band shapes for conjugated molecules.<sup>42</sup> Isegawa and Truhlar showed that the TDA overestimates excitation energies as compared to TDDFT, but the average absolute error changes insignificantly.<sup>43</sup> According to the systematic evaluations, the TDA performs better than the TDDFT in calculation of nonadiabatic couplings between ground and excited states. The correlation between TDDFT and TDA is good when hybrid functionals are used.<sup>43</sup> Some discrepancies between TDDFT and TDA are observed for insulators, while for semiconductors they are negligibly small.<sup>38</sup> Overall, the TDA is a safe way to simplify the original TDDFT formulation.<sup>44</sup> Frontier molecular orbitals and molecular structures were visualized using the open-source molecular builder and visualizer Avogadro.<sup>45,46</sup>

## 2.2 Simplified TDA (sTDA).

It is known that TDA-DFT approach is practical for medium-sized systems.<sup>42</sup> However, its applicability to systems with more than 5000 basis functions is extremely time-consuming. For the large systems, high density of electronic states exist already at common energies. The latter, in turn, can lead to unstable operation of the Davidson algorithm. Introduced recently by Grimme, sTDA method<sup>47</sup> (simplified TDA) was used for characterization of the excited state properties of the studied systems. It solves the majority of problems by introducing basic approximations to the standard TDA-DFT treatment. sTDA employs atom-centered Löwdin-monopole based two-electron repulsion integrals with the asymptotically correct  $1/R$  behavior and perturbative single excitation configuration selection. The sTDA excitation energies are of good quality with typical deviations of 0.2–0.3 eV from experimental data available for EXC26<sup>47</sup> and DYE12<sup>48</sup> benchmark sets. The method was formulated for conventional hybrid functionals but works also good with long-range corrected/range-separated functionals.<sup>49</sup> sTDA method comprises 3 global fit parameters and depends on the amount of Fock-exchange mixing parameter ( $a_x$ ) of density functional. The adaptation of  $a_x$  parameter, responsible for non-local Fock-exchange, is necessary for a particular type of systems. TDA-DFT calculations for  $[\text{Li}@\text{C}_{60}@\text{C}_{240}]^+$  were used as a reference for energetics. We have found that the best performance for the Li-doped CNO systems can be obtained with  $a_x = 0.19$ . Comparison of spectra obtained with TDA-DFT approach and sTDA (with parameters:  $a_x = 0.19$ ,  $\alpha = 0.90$ ,  $\beta = 1.86$ ) demonstrated the excellent performance of the latter. To be completely confident in sTDA performance, the energies of the first singlet excited state of  $[\text{Li}@\text{C}_{60}@\text{C}_{540}]^+$  and  $[\text{Li}@\text{C}_{240}@\text{C}_{540}]^+$  obtained with TDA-DFT and sTDA approaches were compared. According to the TDA-DFT method, the lowest singlet excited state in

$[\text{Li}@\text{C}_{60}@\text{C}_{540}]^+$  complex corresponds to HOMO-LUMO transition with the energy of 0.87 eV and is characterized by the formation of a charge separated state. The sTDA approach predicts the formation of the complex with the same structure with the energy of  $S_0$ - $S_1$  transition equals to 0.65 eV. Thus, the difference in the predicted energies is 0.22 eV. The first singlet excited state for  $[\text{Li}@\text{C}_{240}@\text{C}_{540}]^+$  complex corresponds also to HOMO-LUMO transition with an energy of 0.67 eV and exhibits charge separated nature. At the same time, sTDA predicts a  $S_0$ - $S_1$  gap of 0.59 eV. Most importantly, sTDA approach reproduces correctly the nature of the CS states in both complexes. In this view, further calculations for all other systems were performed within sTDA method with the set of parameters denoted above.

### 2.3 Analysis of excited states.

The quantitative analysis of exciton delocalization and charge transfer in the donor-acceptor complexes was carried out using a tool suggested recently by Plasser *et al.*<sup>50,51</sup> A key quantity is the parameter  $\Omega$ :

$$\Omega(A, B) = \frac{1}{2} \sum_{\alpha \in A, \beta \in B} \left[ \left( \text{SP}^{0i} \right)_{\alpha\beta} \left( \text{P}^{0i} \text{S} \right)_{\alpha\beta} + \text{P}_{\alpha\beta}^{0i} \left( \text{SP}^{0i} \text{S} \right)_{\alpha\beta} \right] \quad (1)$$

$$\text{X}(F_i) = \sum_{A \in F_i} \Omega(A, A) \quad (2)$$

$$\Delta q(\text{CT}^{F_i \rightarrow F_j}) = \sum_{A \in F_i, B \in F_j} \Omega(A, B) + \Omega(B, A) \quad (3)$$

$$\Delta q(\text{CS}^{F_i \rightarrow F_j}) = \sum_{A \in F_i, B \in F_j} \Omega(A, B) - \Omega(B, A) \quad (4)$$

where A and B are atoms,  $F_i$  and  $F_j$  are fragments,  $\alpha$  and  $\beta$  are atomic orbitals,  $\text{P}^{0i}$  is the transition density matrix for the  $\psi_0 \rightarrow \psi_i$  excitation, and S is the overlap matrix.  $\text{X}(F_i)$  is the extent of exciton

localization on the site  $F_i$ .  $\Delta q(CT^{F_i \rightarrow F_j})$  is the total amount of the electron density transferred between the fragments in the  $\psi_0 \rightarrow \psi_i$  excitation.  $\Delta q(\text{CS})$  is a measure of the charge separation between fragments  $F_i$  and  $F_j$ . Note that in the situation when charge transfer  $F_i \rightarrow F_j$ ,  $\delta q$ , is equal to the back transfer  $F_j \rightarrow F_i$ , charge separation between the fragments  $\Delta q(\text{CS}^{F_i \rightarrow F_j})$  is equal to zero, whereas  $\Delta q(CT^{F_i \rightarrow F_j})$  is equal  $2 \cdot \delta q$ .

### 3. RESULTS AND DISCUSSION

First, we consider concentric symmetric complexes,  $C_{60}@C_{240}$ ,  $C_{60}@C_{540}$ ,  $C_{60}@C_{960}$ ,  $C_{240}@C_{540}$ ,  $C_{240}@C_{960}$ , and  $C_{540}@C_{960}$ , and their  $\text{Li}^+$  derivatives. For the smallest species  $C_{60}@C_{240}$ , the interaction energy is found to be -170.5 kcal/mol, which agrees well with previous estimates by Lein<sup>28</sup> and Saielli<sup>26</sup> obtained by different DFT functionals. The stabilization energy of complexes decreases dramatically as the size of the outer shell increases. For  $C_{60}@C_{540}$  and  $C_{60}@C_{960}$ , the energies are -17.6 and -4.0 kcal/mol, respectively. A similar situation is observed for  $C_{240}@C_{540}$  and  $C_{240}@C_{960}$ . Their interaction energies are -490.5 and -52.6 kcal/mol, see Table 1. Interestingly, doping of these systems by  $\text{Li}^+$  leads to a noticeable stabilization associated with a superadditive effect similar to that found for the triple-layered CNOs.<sup>27</sup> The stabilization energy in  $[\text{Li}@C_{60}@C_{240}]^+$  is by almost 8 kcal/mol larger than the sum of the energies in the individual species  $[\text{Li}@C_{60}]^+$  and  $C_{60}@C_{240}$ . As expected, this effect decreases rapidly with increasing size of the outer shell (Table S1).

**Table 1.** Interaction energies ( $\Delta E_{\text{int}}$ , kcal/mol)<sup>a</sup> between CNOs layers obtained at CAM-B3LYP-D3(BJ)/6-31G(d) level of theory.

Outer shell Inner shell	C <sub>240</sub>	C <sub>540</sub>	C <sub>960</sub>
C <sub>60</sub>	-170.46	-17.57	-4.02
Li <sup>+</sup> @C <sub>60</sub>	-208.48	-49.09	-34.69
C <sub>240</sub>	-	-490.46	-52.60
Li <sup>+</sup> @C <sub>240</sub>	-	-503.64	-61.24
C <sub>540</sub>	-	-	-973.96
Li <sup>+</sup> @C <sub>540</sub>	-	-	-979.76

<sup>a</sup> Interaction energies were calculated as a difference in electronic energies for particular CNO and energies of its individual fragments.

Excited state properties of C<sub>60</sub>@C<sub>240</sub> were previously studied using the semiempirical INDO/S method.<sup>29</sup> It was shown that charge-separated states in this model lie higher in energy than locally excited states, and thus have a very short lifetime. However, it should be noted that INDO/S and many others semiempirical methods provide very inaccurate vertical IP and EA values that can lead to significant errors in the description of charge separated (CS) processes (Tables S2 – S4). Thus, using DFT methods for the description of ionization potentials is strictly required.

Since the energy of locally excited states is defined mainly by the HOMO-LUMO (H-L) gap, we have checked how the H-L gap depends on the DFT functionals used. For this aim, we have compared our data obtained by CAM-B3LYP with values computed using the PBE0 hybrid functional.<sup>24</sup> We have found that the H-L gap values obtained by the range-separated CAM-B3LYP functional is more than 1 eV bigger as compared to those obtained with the PBE0 functional (Table S5). At the same time, comparison of HOMO energies obtained by CAM-

B3LYP and PBE0 functionals with experimental vertical ionization potential values (Table S3) allows us to state that CAM-B3LYP provides more reliable results.

The lowest 80 singlet excited states of  $[\text{Li}@\text{C}_{60}@\text{C}_{240}]^+$  lie in the range of 1.703 – 2.788 eV. The oscillator strength ( $f$ ) of the electronic transitions is quite weak, with  $f_{\text{max}} = 0.166$ . The energies of 80 triplets are found in the range of 1.633 – 2.630 eV. Both charge shift and locally excited (LE) states are identified (see Table 2). Interestingly, 30 lowest singlets are the CS states. 22 lowest singlet excited states (1.703 – 2.152 eV) correspond to dipole-forbidden transitions ( $f$  is equal to zero) with a large charge shift ranging from 0.77 to 0.93e. By the excitations, the electron density is transferred from  $\text{C}_{240}$  to  $\text{C}_{60}$ . The generated states,  $\text{Li}^+@\text{C}_{60}^-@\text{C}_{240}^+$ , can be described as a molecular capacitor with the oppositely charged external and internal fullerenes. The negative charge is delocalized over  $\text{C}_{60}$ , whereas the positive charge is located on  $\text{C}_{240}$ . Taking into account that  $[\text{Li}@\text{C}_{60}@\text{C}_{240}]^+$  system exhibits  $I_h$  symmetry, HOMOs are 5-fold degenerated, while LUMOs are 3-fold degenerated and exhibit  $\pi$ -nature. All 30 lowest CS states correspond to the transitions from HOMO to LUMO or LUMO+1, which allowed us to assign these transitions as  $\pi \rightarrow \pi^*$ . Three transitions at 2.158 eV are CS states with a charge shift of 0.95e. They are of particular interest because can be directly populated by light absorption (the total oscillator strength is 0.17). Five states at 2.202 eV are the CS states.

**Table 2.** Electronic properties of singlet excited states of  $C_{60}@C_{240}$  and  $[Li@C_{60}@C_{240}]^+$  computed by TDA-CAM-B3LYP. X – exciton localization and  $\Delta q(\text{CS})$  – charge shift between the  $C_{60}$ ,  $C_{240}$  or Li sites.<sup>a</sup>

Energy range (eV)	Type	Associated fragment	N <sup>c</sup>	X( $C_{240}$ ), au	X( $C_{60}$ ), au	$\Delta q(\text{CS})^d$ , e
<b><math>C_{60}@C_{240}</math></b>						
2.196 – 2.403	LE	$C_{240}$	13	0.89	0.02	0.10
2.489	Mix	$C_{60}^{\delta-}@C_{240}^{\delta+}$	5			0.31
2.538 – 2.587	LE	$C_{240}$	12	0.92	0.00	0.04
2.591 – 2.617	LE	$C_{60}$	7	0.10	0.74	0.06
2.804 – 2.853	CS	$C_{60}^-@C_{240}^+$	10			0.69
2.880 – 2.939	Mix	$C_{60}^{\delta-}@C_{240}^{\delta+}$	10			0.19
<b>2.950 (2.648)<sup>b</sup></b>	Mix	$C_{60}^{\delta-}@C_{240}^{\delta+}$	3	0.48	0.02	0.46
2.968	LE	$C_{60}$	5	0.01	0.49	0.08
<b>2.978–3.137 (0.740)<sup>b</sup></b>	Mix	$C_{60}^{\delta-}@C_{240}^{\delta+}$	14			0.22
3.142	LE	$C_{240}$	1	0.95	0.00	0.00
<b><math>Li@C_{60}@C_{240}</math></b>						
1.703–2.152	CS	$Li^+@C_{60}^-@C_{240}^+$	22	0.05–0.21	0.01	0.77–0.93
<b>2.158 (0.166)<sup>b</sup></b>	CS	$Li^+@C_{60}^-@C_{240}^+$	3	0.04	0.01	0.95
2.202	CS	$Li^+@C_{60}^-@C_{240}^+$	5	0.12	0.01	0.88
2.341–2.396	LE	$C_{240}$	10	0.91	0.01	0.08
2.460–2.582	CS	$Li^+@C_{60}^-@C_{240}^+$	15	0.29–0.43	0.01	0.57–0.70
2.651	LE	$C_{60}$	3	0.00	0.93	0.01
2.657	Mix	$Li^+@C_{60}^{\delta-}@C_{240}^{\delta+}$	3	0.67	0.00	0.32

2.687–2.709	LE	C <sub>240</sub> and C <sub>60</sub>	13			0.01
2.717	Mix	Li <sup>+</sup> @C <sub>60</sub> <sup>δ-</sup> @C <sub>240</sub> <sup>δ+</sup>	5	0.61	0.00	0.38
2.788 <sup>d</sup>	CS	Li@C <sub>60</sub> @C <sub>240</sub> <sup>+</sup>	1	0.01	0.01	0.95

<sup>a</sup> The quantities X and Δq(CS) are defined by Eqs. 2 and 4, respectively. <sup>b</sup> Oscillator strength greater than 10<sup>-4</sup> are shown in parentheses. <sup>c</sup> N – number of excited states in the given energy range. <sup>d</sup> CS occurs from C<sub>240</sub> to C<sub>60</sub> moieties in all listed transitions except for excited state of 2.788 eV, where positive charge shifts from Li<sup>+</sup> to C<sub>240</sub>.

Ten transitions at 2.341 – 2.396 eV are localized on C<sub>240</sub> and have zero oscillator strengths. Transitions with exciton localization on C<sub>60</sub> are found at 2.651 eV. Twenty-one transitions in the range of 2.657 – 2.717 eV are also locally excited states. Several mixed states in this intermediate region exhibit partial charge shift (Δq is 0.32 – 0.38). Finally, the state at 2.788 eV corresponds to a new type of CS states, where the electron is transferred from C<sub>240</sub> to Li<sup>+</sup> moiety and characterized by Δq(CS) equals to 0.95e. Thereby, generation of the Li@C<sub>60</sub>@C<sub>240</sub><sup>+</sup> complex is observed. This CS state is associated with the transition from HOMO to LUMO+3 orbitals. Detachment orbital corresponds to π type, while attachment orbital is almost completely localized on the Li atom and corresponds to the σ type.

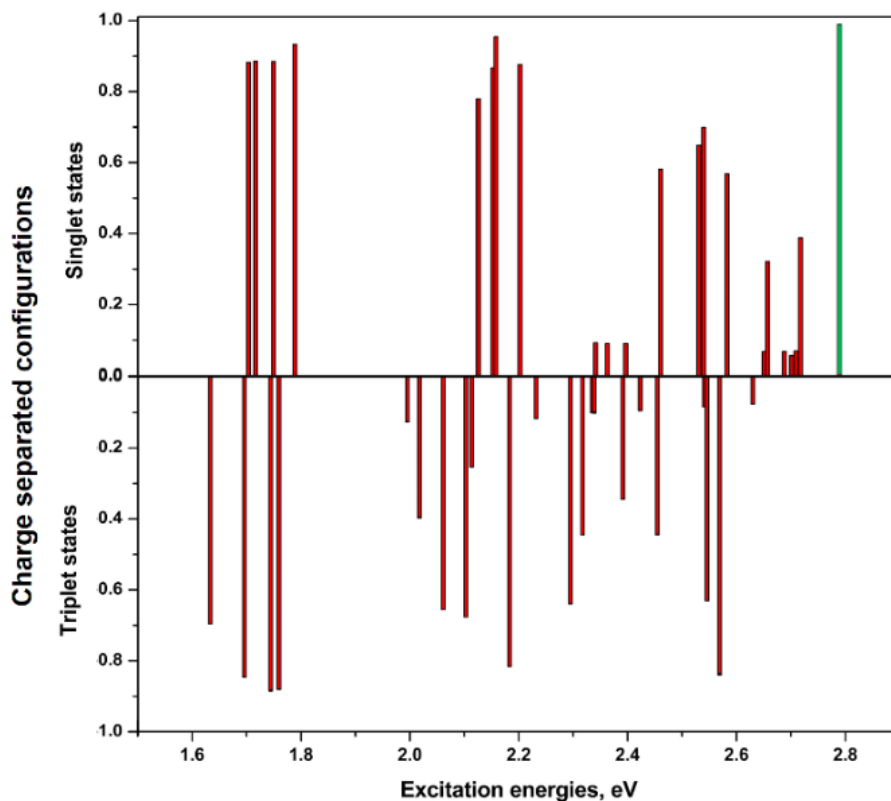


**Figure 1.** Photoinduced charge separated states for  $[\text{Li}@\text{C}_{60}@\text{C}_{240}]^+$  in singlet and triplet excited states. Red bars correspond to complex with structure  $\text{Li}^+@\text{C}_{60}^-\text{C}_{240}^+$ ; green bar –  $\text{Li}^0@\text{C}_{60}^0@\text{C}_{240}^+$ . Charges are in electrons.

Analysis of 80 triplet excited states shows that the low-lying states correspond to the CS states. They are very similar to the corresponding singlet excited states, where the electron is transferred from  $\text{C}_{240}$  to  $\text{C}_{60}$  fragment (Table S6). The CS states for the  $\text{Li}^+@\text{C}_{60}@\text{C}_{240}$  complex are shown in Figure 1. The lowest singlet and triplet state energies are very similar, *e.g.* the  $\text{S}_1$  and  $\text{T}_1$  states are found at 1.703 and 1.633 eV, respectively. The same is also valid for singlets and triplets localized on  $\text{C}_{240}$ . However, LE triplet states of  $\text{C}_{60}$  are by 0.20 eV lower in energy than the singlets. No  $\text{Li}@\text{C}_{60}@\text{C}_{240}^+$  states were found within the studied 80 low-lying triplets.

For a better understanding of the  $\text{Li}^+$  doping effect, comparison of the excited states properties of  $\text{Li}^+$ -doped system with pure  $\text{C}_{60}@\text{C}_{240}$  has been performed. According to TDA-CAM-B3LYP calculations, the considered 80 excited states of  $\text{C}_{60}@\text{C}_{240}$  are located in the range of 1 eV, with the lowest excited state characterized by the energy value of 2.20 eV. Nature of the 1<sup>st</sup> excited state can be characterized as locally excited state located mainly on the  $\text{C}_{240}$  fragment. Next several absorptive states were detected in the range of 2.95-3.14 eV (Table 2). In all cases, exciton is localized at the  $\text{C}_{240}$  moiety. In the studied energy range (1 eV/ 80 excited states), CT states with other nature were not found. Thus, doping of the  $\text{C}_{60}@\text{C}_{240}$  system with  $\text{Li}^+$  leads not only to a notable red shift of the absorption spectra (by *ca.* 0.5 eV), but also to significant stabilization of CT form (by *ca.* 0.8 eV). Moreover, the magnitude of charge separation in CT states in  $[\text{Li}@\text{C}_{60}@\text{C}_{240}]^+$  becomes larger compared to  $\text{C}_{60}@\text{C}_{240}$  system. At the same time, the effect of  $\text{Li}^+$  dopant on the positions of LE states located on both  $\text{C}_{240}$  and  $\text{C}_{60}$  fragments can be rated as minimal (Table 2). The latter allowed us to predict that highly absorptive states of  $[\text{Li}@\text{C}_{60}@\text{C}_{240}]^+$  complex should be located at 2.90-3.00 eV energy range, similarly to the original  $\text{C}_{60}@\text{C}_{240}$  system.

For the prediction of the excited states energies for giant CNOs, the sTDA method was used. It was pre-calibrated according to TDA-DFT data in the way to reproduce the CS energies in  $[\text{Li}@\text{C}_{60}@\text{C}_{240}]^+$  complex. The configuration space was restricted to 3 eV. Figure 2 demonstrates energetic diagram for the ground and first singlet excited state, as well as the frontier molecular orbitals (HOMO-LUMO) of the studied system.

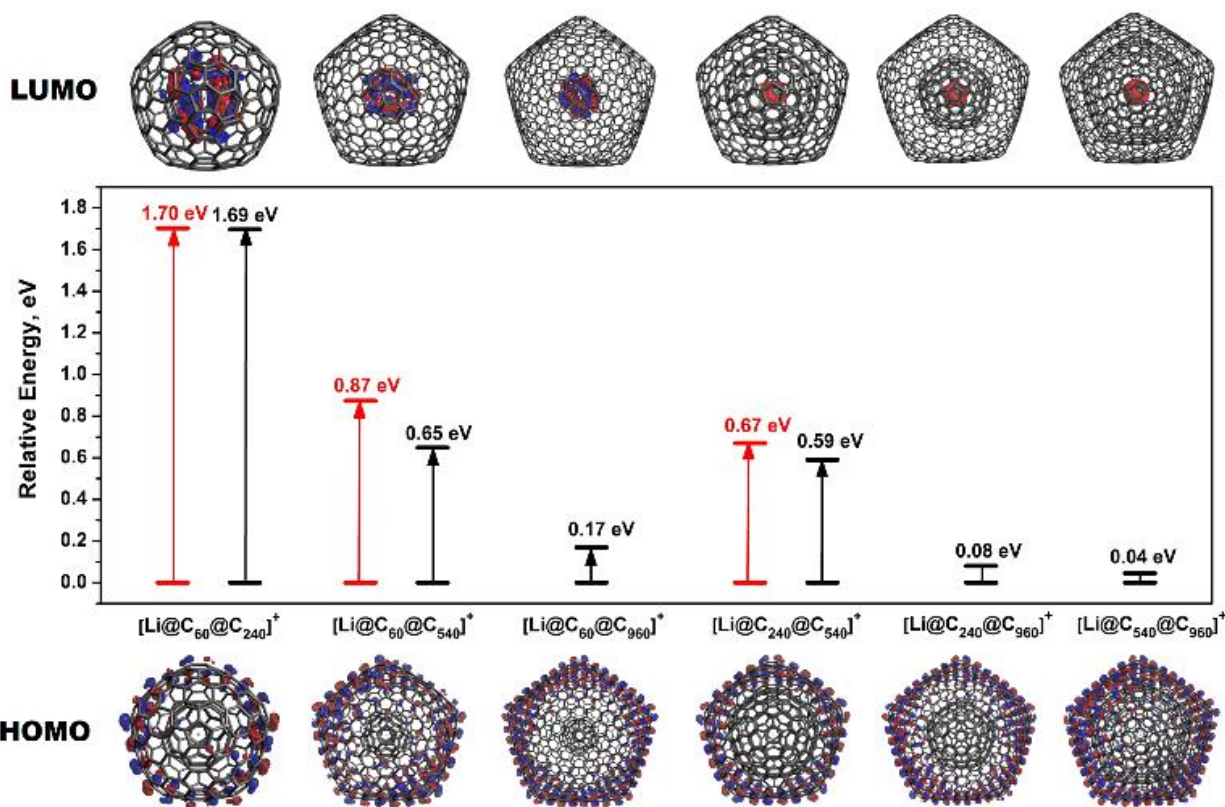


**Figure 2.** Frontier molecular orbitals (HOMO, LUMO) and relative energies of ground and first excited states, which in all cases correspond to HOMO→LUMO transition associated with charge transfer from the outer shell to inner fragment. The red and black lines show the energies computed with CAM-B3LYP/6-31G\* and sTDA, respectively.

In the large systems, the lowest excited states correspond to CS excitations as in the smallest  $[\text{Li}@C_{60}@C_{240}]^+$  complex. The analysis of excited state energies and molecular orbitals revealed two interesting features. First, the CS character of the first excited state depends on the size of the inner shell. If the inner shell is  $C_{60}$ , the  $S_1$  state is of the capacitor-like type,  $\text{Li}^+@C_{60}^-@C_{YYY}^+$ , which is generated by ET from the outer shell to the inner shell. However, the nature of the lowest CS states will change when the size of the encapsulated cage increases. For the complexes  $[\text{Li}@C_{240}@C_{540}]^+$ ,  $[\text{Li}@C_{240}@C_{960}]^+$ , and  $[\text{Li}@C_{540}@C_{960}]^+$ , the ET occurs from the outer shell to

$\text{Li}^+$  with the formation of  $\text{Li}@@\text{C}_{\text{XXX}}@\text{C}_{\text{YYY}}^+$  state. This switch between the two types of states results from the change of the LUMO character of  $\text{Li}^+@\text{C}_{\text{XXX}}@\text{C}_{\text{YYY}}$  that is located in the inner-cage for small inner fullerenes and in the  $\text{Li}^+$  for large inner fullerenes. Thus, for the systems where  $\text{Li}^+$  is encapsulated into  $\text{C}_{240}$  and higher fullerenes,  $\text{Li}^+$  becomes a stronger electron acceptor than the cage.

These results can be explained as follows. In the considered complexes, two types of CS states exist: CS1,  $\text{Li}@\text{X}@\text{Y}^+$ , formed by ET from outer shell Y to  $\text{Li}^+$ , and CS2,  $\text{Li}^+@\text{X}^-\text{Y}^+$ , generated by charge separation between X and Y. We consider the ground state,  $\text{Li}^+@\text{X}@\text{Y}$ , as a reference. CS1 is generated when 1 electron is fully transferred from the outer shell Y to  $\text{Li}^+$ , and its energy is determined by the difference in the ionization potentials ( $IP$ ) of the outer shell Y and the Li atom.

$$E_{CS1} = IP(Y) - IP(Li) \quad (5)$$

The CS(2) energy is determined by eq. (6)

$$E_{CS2} = IP(Y) - EA(X) + \frac{q(X)q(Li)}{R_X} + \frac{q(Y)q(Li)}{R_Y} + \frac{q(X)q(Y)}{R_Y} \cong IP(Y) - EA(X) - \frac{14.4}{R_X} \quad (6)$$

Here,  $IP(Y)$  is the ionization potential of the shell Y,  $EA(X)$  is the electron affinity ( $EA$ ) of the inner shell X. Last 3 terms correspond to electrostatic interactions of the charges on X ( $q(X)=-1$ ), Y ( $q(Y)=1$ ), and Li ( $q(Li)=1$ ).  $R_X$  and  $R_Y$  are the effective radii of the inner and outer shells in Å. All energies are in eV.

The sign of the energy difference of CS1 and CS2,  $\Delta = E_{CS2} - E_{CS1}$ , indicates which state of the two CS states will be generated.

$$\Delta = IP(Li) - EA(X) - \frac{14.4}{R_X} \quad (7)$$

The  $IP$ ,  $EA$ ,  $R$  and  $\Delta$  values for  $C_{60}$ ,  $C_{240}$ , and  $C_{540}$  are listed in Table 3. We note that  $\Delta$  in Eq. (7) depends only on internal part of the system ( $IP$  of encapsulated metal,  $EA$  and radius of the inner shell).

**Table 3.** Vertical ionization potentials and electron affinities ( $IP$  and  $EA$ ) for selected fragments, average radii ( $R$ ) of outer and inner shells, CS1 and CS2 energies for  $[Li@C_{60}@C_{240}]^+$  and  $[Me@C_{240}@C_{540}]^+$  ( $Me=Li, Cs$ ). All energies are in eV.

Frag.	$IP$	$EA$	$R^a, \text{\AA}$	$[Li@C_{60}@C_{240}]^+$	$[Li@C_{240}@C_{540}]^+$	$[Cs@C_{240}@C_{540}]^+$
Li	5.59			$\Delta^b = -0.24$	$\Delta^b = 1.17$	$\Delta^b = -0.50$
Cs	3.92					
$C_{60}$		1.76	3.537			
$C_{240}$		2.38	7.051			
$C_{540}$		2.82	10.520			

<sup>a</sup> determined as the mean distance between each atom and the centre of the shell; <sup>b</sup>  $\Delta = E_{CS2} - E_{CS1}$

The negative  $\Delta$  found for  $[Li@C_{60}@C_{240}]^+$  suggests that the CS2 is its lowest excited state. In turn, the positive  $\Delta$  for  $[Li@C_{240}@C_{540}]^+$  means that the CS1 state will be generated first. These predictions are in good agreement with the TDDFT calculations.

Eq. 7 can be generalized for arbitrary systems  $Me@X@Y$ , where  $X$  is a Goldberg-type fullerene  $C_N$  ( $N=60 \cdot m^2$ ,  $m=1, 2, 3 \dots$ ).

$$\Delta = IP(Me) - 0.475(\ln N + 67N^{-\frac{1}{2}} - 0.42), \quad (8)$$

where  $IP(Me)$  is the ionization potential of the encapsulated species (in our systems,  $Me = Li$ ), and  $N$  is the number of carbon atoms in the inner shell. The second term in Eq. (8) describes the derived dependence of  $EA(X)$  and  $R_X$  on  $N$  (the size of the inner shell  $X$ ).

To check the proposed expression for prediction of the type of lowest CS transition in nested fullerenes  $\text{Me}@X@Y$ , let us compare two CNOs:  $[\text{Li}@C_{240}@C_{540}]^+$  and  $[\text{Cs}@C_{240}@C_{540}]^+$ . In line with Eq. (8), the nature of CS in these systems should be different. In  $[\text{Li}@C_{240}@C_{540}]^+$ ,  $\Delta$  is equal to 1.17 eV (Table 3) and the lowest CT transition corresponds to ET from the outer shell to  $\text{Li}^+$ . A negative value of  $\Delta$  found for  $[\text{Cs}@C_{240}@C_{540}]^+$ ,  $\Delta=-0.50$  eV, suggests the alternative type of CS where an electron is transferred between the outer and inner shells. To verify this result, we performed TDA calculations of  $[\text{Cs}@C_{240}@C_{540}]^+$ . The analysis of the lowest excited state in this latter system shows that the CS state is formed by ET between the shells. In contrast, TDA calculations of  $[\text{Li}@C_{240}@C_{540}]^+$  predict that the lowest CS in this complex is generated by ET from the outer shell to  $\text{Li}^+$ . Thus, Eq. (8) allows one to predict correctly the type of the lowest CS state in the doped double-layered CNOs. Note that the energy of the CS state in  $[\text{Li}@C_{240}@C_{540}]^+$  (0.67 eV), differs substantially from that in  $[\text{Cs}@C_{240}@C_{540}]^+$  (1.62 eV). The frontier molecular orbitals representing the lowest excited states in  $\text{Li}^+$  and  $\text{Cs}^+$  doped systems are shown in Figure S2, SI.

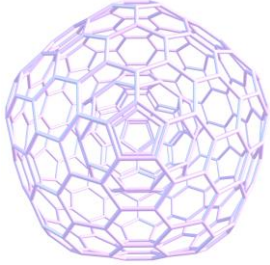
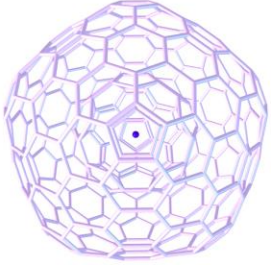
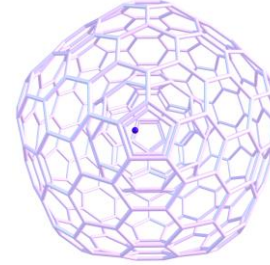
As expected, the HOMO-LUMO energy gap in double-layered CNOs is quite sensitive to the size of systems. For the smallest CNO,  $[\text{Li}@C_{60}@C_{240}]^+$ , the energy gap is found to be 1.70 eV, whereas very small gaps were found in the large complexes,  $[\text{Li}@C_{240}@C_{960}]^+$  and  $[\text{Li}@C_{540}@C_{960}]^+$  (0.09 and 0.05 eV, respectively). Such small gaps may lead to metallic-like properties of the systems. Fig. 2 demonstrates a qualitative trend in HOMO-LUMO gap. Overall, the energy gap can easily be tuned by varying both the encapsulated metal ion and the size of the external shell.

### *Effect of the Li<sup>+</sup> ion encapsulation*

As demonstrated above, the encapsulation of Li<sup>+</sup> ion leads to considerable changes in the electronic structure of CNOs. In particular, the energy gap decreases dramatically. In C<sub>60</sub>@C<sub>240</sub>, the energy gap between GS and CS reduces from 2.20 to 1.70 eV (Table 4). This can be explained as follows. In neutral (undoped) complexes, the lowest excited state is the LE state localized on the C<sub>240</sub> moiety. Their HOMO and LUMO orbital energies, as well as the energy of LE states are almost identical to those in isolated C<sub>240</sub>, because orbital interaction between the shells is weak. In contrast, in the Li<sup>+</sup> derivative the lowest excited state is the CS state with electron and hole localized on C<sub>60</sub> and C<sub>240</sub>, respectively. As expected, the energy of LE states is almost insensitive to Li<sup>+</sup> (Table 4). When passing from C<sub>60</sub>@C<sub>240</sub> to [Li@C<sub>60</sub>@C<sub>240</sub>]<sup>+</sup>, the energy of LE (C<sub>240</sub>) changes only by 0.15 eV, whereas LE (C<sub>60</sub>) changes by 0.09 eV. However, the energy of the CS state corresponding to electron transfer from the outer shell to the inner shell changes by more than 1 eV.

Because of different nature of the first excited states in doped and undoped species, a great change in energy gap is observed. Additionally, we checked the effect of Li<sup>+</sup> location on excited state electronic properties of the [Li@C<sub>60</sub>@C<sub>240</sub>]<sup>+</sup> complex. Conformer with Li<sup>+</sup> located not in the center of fullerenes is more stable compared to the centered one by 4.7 kcal/mol. As can be seen from Table 4, the electronic properties (energetics of LE and CT states) for both conformers are nearly identical. Therefore, all the systems studied in this work have been considered with icosahedral symmetry to reduce the computational cost.

**Table 4.** Electronic properties of singlet excited states (in eV) of  $C_{60}@C_{240}$  in centered and uncentered  $[Li@C_{60}@C_{240}]^+$  computed with the TDA-CAM-B3LYP method.

			
	$C_{60}@C_{240}$	$[Li@C_{60}@C_{240}]^+$ centered	$[Li@C_{60}@C_{240}]^+$ uncentered
LE ( $C_{240}$ )	2.196	2.341	2.336
LE( $C_{60}$ )	2.560	2.651	2.601
CS ( $C_{60}^-@C_{240}^+$ )	2.804	1.703	1.668
HOMO( $C_{240}$ )	-6.356	-8.206	-8.204
LUMO ( $C_{240}$ )	-2.705	-4.402	-4.409
HOMO( $C_{60}$ )	-7.191	-9.944	-9.888
LUMO ( $C_{60}$ )	-2.180	-5.097	-5.137

Note that the energies of the orbitals localized on the inner ( $C_{60}$ ) and outer ( $C_{240}$ ) spheres decrease by  $\sim 3$  and  $2$  eV, correspondingly (see data for HOMO and LUMO in Table 4). The shifts can be approximately estimated as  $14.4 \frac{Q}{R}$  eV, where  $Q$  is the charge on the metal and  $R$  is the radius of the sphere in Å.

An alternative explanation of small adiabatic gap for  $Li^+$ -doped CNOs can also be provided. For a weakly interacting donor and acceptor (D-A) system, the adiabatic gap ( $\Delta E$ ) is defined by the

energy of isolated donor and acceptor ( $\varepsilon_D$  and  $\varepsilon_A$ ), and the electronic coupling ( $V_{DA}$ ) of the diabatic states:<sup>52</sup>

$$\Delta E^2 = (\varepsilon_D - \varepsilon_A)^2 + 4V_{DA}^2 \quad (9)$$

In the case where the diabatic states are nearly degenerated ( $\varepsilon_D \approx \varepsilon_A$ ), the adiabatic gap is defined by  $V_{DA}$

$$\Delta E = 2|V_{DA}| \quad (10)$$

It was previously shown that depending on the character of the diabatic states, the electronic coupling in CNOs is in the region of 0.001 – 0.1 eV.<sup>29</sup> Thus, change in the character of the lowest excited state due to inserting of  $\text{Li}^+$  ion may lead to a small gap value when the donor and acceptor states have similar energies.

## CONCLUSIONS

The excited state properties of six double-layered CNOs and their  $\text{Li}^+$  doped derivatives have been studied in detail using TDDFT and sTDA methods. We have shown that the lowest excited states of the  $\text{Li}^+$ -containing systems correspond to charge separated states. Two types of the CT states have been identified: (1) states with alternating charges in CNOs containing the  $\text{C}_{60}$  as inner shell, e.g.  $\text{Li}^+@\text{C}_{60}^-\text{C}_{240}^+$ , and (2) states with a positive charge on the outer shell in CNOs with a bigger inner shell, e.g. in  $\text{Li}@\text{C}_{240}\text{C}_{540}^+$ . This switch between the two types of CS states results from the interchange of the LUMO localized on the inner cage and  $\text{Li}^+$ . We have suggested a simple expression to estimate the energy difference in these states and thus to predict the type of the lowest CS state in the nested fullerenes  $[\text{Me}@\text{X}@\text{Y}]^+$ :  $\Delta = IP(\text{Me}) - 0.475(\ln N + 67N^{-\frac{1}{2}} - 0.42)$ .

## ASSOCIATED CONTENT

### Supporting Information

Table S1 lists the formation energy of the CNOs, the interaction energies between the CNOs layers and the superadditivity energies. Comparison of electronic properties calculated by semiempirical methods and TDA-DFT is given in Tables S2-S4. Table S5 shows the HOMO-LUMO gap in the CNOs. Electronic properties of triplet excited states of  $[\text{Li}@\text{C}_{60}@\text{C}_{240}]^+$  are merged in Table S6. The calculated absorption spectra for  $\text{C}_{60}@\text{C}_{240}$  and  $[\text{Li}@\text{C}_{60}@\text{C}_{240}]^+$  are shown in Figure S1. Figure S2 illustrates the frontier molecular orbitals for  $[\text{Li}@\text{C}_{240}@\text{C}_{540}]^+$  and  $[\text{Cs}@\text{C}_{240}@\text{C}_{540}]^+$ . This material is available free of charge via the Internet at <http://pubs.acs.org>.

## AUTHOR INFORMATION

### Corresponding Author

\* E-mail: [antony.stasuk@gmail.com](mailto:antony.stasuk@gmail.com) (Anton J. Stasyuk)

\* E-mail: [miquel.sola@udg.edu](mailto:miquel.sola@udg.edu) (Miquel Solà)

\* E-mail: [alexander.voityuk@icrea.cat](mailto:alexander.voityuk@icrea.cat) (Alexander A. Voityuk)

### Funding Sources

This project has received funding support from the Spanish MINECO (Network CTQ2016-81911-REDT, projects CTQ2017-85341-P and CTQ2015-69363-P, and Juan de la Cierva formación contracts FJCI-2016-29448 to A.J.S. and FJCI-2017-32757 to O.A.S.), the Catalan DIUE

(2017SGR39, XRQTC, and ICREA Academia 2014 Award to M.S.), and the FEDER fund (UNGI10-4E-801).

## Notes

The authors declare no competing financial interest.

## ACKNOWLEDGEMENTS

A. J. S. gratefully acknowledges The Interdisciplinary Centre for Mathematical and Molecular Modelling of the University of Warsaw (ICM) for computational facilities (grant no. G33-17).

## ABBREVIATIONS

CNO - carbon nano-onion; IPR - Isolated Pentagon Rule; CS - charge separated; ET - electron transfer; sTDA - simplified TDA; LE - locally excited; IP - ionization potential; EA - electron affinity.

## REFERENCES

- (1) Suarez-Martinez, I.; Grobert, N.; Ewels, C. P. Nomenclature of  $sp^2$  carbon nanoforms. *Carbon* **2012**, *50*, 741-747.
- (2) Iijima, S. Direct observation of the tetrahedral bonding in graphitized carbon black by high resolution electron microscopy. *J. Cryst. Growth*. **1980**, *50*, 675-683.
- (3) Ugarte, D. Curling and closure of graphitic networks under electron-beam irradiation. *Nature* **1992**, *359*, 707-709.

- (4) Mordkovich, V. Z.; Umnov, A. G.; Inoshita, T. Nanostructure of laser pyrolysis carbon blacks: observation of multiwall fullerenes. *Int. J. Inorg. Mater.* **2000**, *2*, 347-353.
- (5) He, C.; Zhao, N.; Shi, C.; Du, X.; Li, J. Carbon nanotubes and onions from methane decomposition using Ni/Al catalysts. *Mater. Chem. Phys.* **2006**, *97*, 109-115.
- (6) McDonough, J. K.; Gogotsi, Y. Carbon Onions: Synthesis and Electrochemical Applications. *Electrochem. Soc. Interface.* **2013**, *22*, 61-66.
- (7) Xiao, J.; Ouyang, G.; Liu, P.; Wang, C. X.; Yang, G. W. Reversible Nanodiamond-Carbon Onion Phase Transformations. *Nano Lett.* **2014**, *14*, 3645-3652.
- (8) Kuznetsov, V. L.; Chuvilin, A. L.; Butenko, Y. V.; Mal'kov, I. Y.; Titov, V. M. Onion-like carbon from ultra-disperse diamond. *Chem. Phys. Lett.* **1994**, *222*, 343-348.
- (9) Fan, J.-C.; Sung, H.-H.; Lin, C.-R.; Lai, M.-H. The production of onion-like carbon nanoparticles by heating carbon in a liquid alcohol. *J. Mater. Chem.* **2012**, *22*, 9794-9797.
- (10) Huang, J. Y.; Yasuda, H.; Mori, H. Highly curved carbon nanostructures produced by ball-milling. *Chem. Phys. Lett.* **1999**, *303*, 130-134.
- (11) Sano, N.; Wang, H.; Chhowalla, M.; Alexandrou, I.; Amaratunga, G. A. J. Synthesis of carbon 'onions' in water. *Nature* **2001**, *414*, 506-507.
- (12) Bushueva, E.G.; Galkin, P.S.; Okotrub, A.V.; Bulusheva, L.G.; Gavrilov, N.N.; Kuznetsov, V.L.; et al. Double layer supercapacitor properties of onion-like carbon materials. *Phys. Status Solidi B.* **2008**, *245*, 2296-2299.

(13) McDonough, J. K.; Frolov, A. I.; Presser, V.; Niu, J.; Miller, C. H.; Ubieto, T.; Fedorov, M. V.; Gogotsi, Y. Influence of the structure of carbon onions on their electrochemical performance in supercapacitor electrodes. *Carbon* **2012**, *50*, 3298-3309.

(14) Wang, Y.; Han, Z. J.; Yu, S. F.; Song, R. R.; Song, H. H.; Ostrikov, K.; Yang, H. Y. Core-leaf onion-like carbon/MnO<sub>2</sub> hybrid nano-urchins for rechargeable lithium-ion batteries. *Carbon* **2013**, *64*, 230-236.

(15) Tian, W.; Hu, H.; Wang, Y.; Li, P.; Liu, J.; Liu, J.; Wang, X.; Xu, X.; Li, Z.; Zhao, Q.; Ning, H.; Wu, W.; Wu, M. Metal–Organic Frameworks Mediated Synthesis of One-Dimensional Molybdenum-Based/Carbon Composites for Enhanced Lithium Storage. *ACS Nano* **2018**, *12*, 1990-2000.

(16) Shenderova, O.; Grishko, V.; Cunningham, G.; Moseenkov, S.; McGuire, G.; Kuznetsov, V. Onion-like carbon for terahertz electromagnetic shielding. *Diamond Relat. Mater.* **2008**, *17*, 462-466.

(17) Macutkevicius, J.; Adomavicius, R.; Krotkus, A.; Seliuta, D.; Valusis, G.; Maksimenko, S.; Kuzhir, P.; Batrakov, K.; Kuznetsov, V.; Moseenkov, S.; Shenderova, O.; Okotrub, A. V.; Langlet, R.; Lambin, P. Terahertz probing of onion-like carbon-PMMA composite films. *Diamond Relat. Mater.* **2008**, *17*, 1608-1612.

(18) Mitrajit, G.; Kumar, S. S.; Manav, S.; Sabyasachi, S. Carbon Nano-onions for Imaging the Life Cycle of *Drosophila Melanogaster*. *Small* **2011**, *7*, 3170-3177.

(19) Giordani, S.; Bartelmess, J.; Frasconi, M.; Biondi, I.; Cheung, S.; Grossi, M.; Wu, D.; Echevoyen, L.; O'Shea, D. F. NIR fluorescence labelled carbon nano-onions: synthesis, analysis and cellular imaging. *J. Mater. Chem. B* **2014**, *2*, 7459-7463.

(20) Luszczyn, J.; Polonska-Brzezinska, M.E.; Palkar, A.; Simionescu, A.; Simionescu, D. T.; Kalska-Szostko, B.; Winkler, K.; Echevoyen, L. Small Noncytotoxic Carbon Nano-Onions: First Covalent Functionalization with Biomolecules. *Chem. - Eur. J.* **2010**, *16*, 4870-4880.

(21) Yang, M.; Flavin, K.; Kopf, I.; Radics, G.; Hearnden, C. H. A.; McManus, G. J.; Moran, B.; Villalta-Cerdas, A.; Echevoyen, L. A.; Giordani, S.; Lavelle, E. C. Functionalization of Carbon Nanoparticles Modulates Inflammatory Cell Recruitment and NLRP3 Inflammasome Activation. *Small* **2013**, *9*, 4194–4206.

(22) Giordani, S.; Bartelmess, J.; Frasconi, M.; Biondi, I.; Cheung, S.; Grossi, M.; Wu, D.; Echevoyen, L.; O'Shea, D. F. NIR fluorescence labelled carbon nano-onions: synthesis, analysis and cellular imaging. *J. Mater. Chem. B* **2014**, *2*, 7459–7463.

(23) Bartelmess, J.; De Luca, E.; Signorelli, A.; Baldrighi, M.; Becce, M.; Brescia, R.; Nardone, V.; Parisini, E.; Echevoyen, L.; Pompa, P. P.; Giordani, S. Boron dipyrromethene (BODIPY) functionalized carbon nano-onions for high resolution cellular imaging. *Nanoscale* **2014**, *6*, 13761–13769.

(24) Cadranel, A.; Margraf, J.T.; Strauss, V.; Clark, T.; Guldi, D.M. Carbon nanodots for charge-transfer processes. *Acc. Chem. Res.*, **2019**, *52*, pp 955–963.

(25) Moriyama, R.; Wu, J. W. J.; Nakano, M.; Ohshimo, K.; Misaizu, F. Small Carbon Nano-Onions: An Ion Mobility Mass Spectrometric Study. *J. Phys. Chem. C* **2018**, *122*, 5195-5200.

- (26) Casella, G.; Bagno, A.; Saielli, G. Spectroscopic signatures of the carbon buckyonions  $C_{60}@C_{180}$  and  $C_{60}@C_{240}$ : a dispersion-corrected DFT study. *Phys. Chem. Chem. Phys.* **2013**, *15*, 18030-18038.
- (27) Grimme, S.; Mück-Lichtenfeld, C.; Antony, J. Noncovalent Interactions between Graphene Sheets and in Multishell (Hyper)Fullerenes. *J. Phys. Chem. C* **2007**, *111*, 11199-11207.
- (28) Hashmi, M. A.; Lein, M. Carbon Nano-onions as Photosensitizers: Stacking-Induced Red-Shift. *J. Phys. Chem. C* **2018**, *122*, 2422-2431.
- (29) Voityuk, A. A.; Solà, M. Photoinduced Charge Separation in the Carbon Nano-Onion  $C_{60}@C_{240}$ . *J. Phys. Chem. A* **2016**, *120*, 5798-5804.
- (30) Kamimura, T.; Ohkubo, K.; Kawashima, Y.; Nobukuni, H.; Naruta, Y.; Tani, F.; Fukuzumi, S. Submillisecond-lived photoinduced charge separation in inclusion complexes composed of  $Li^+@C_{60}$  and cyclic porphyrin dimers. *Chem. Sci.* **2013**, *4*, 1451-1461.
- (31) Kawashima, Y.; Ohkubo, K.; Okada, H.; Matsuo, Y.; Fukuzumi, S. Supramolecular Formation of  $Li^+@PCBM$  Fullerene with Sulfonated Porphyrins and Long-Lived Charge Separation. *ChemPhysChem* **2014**, *15*, 3782-3790.
- (32) Hirata, S.; Head-Gordon, M. Time-dependent density functional theory within the Tamm–Dancoff approximation. *Chem. Phys. Lett.* **1999**, *314*, 291-299.
- (33) Yanai, T.; Tew, D. P.; Handy, N. C. A new hybrid exchange–correlation functional using the Coulomb-attenuating method (CAM-B3LYP). *Chem. Phys. Lett.* **2004**, *393*, 51-57.

- (34) Frisch, M. J.; Trucks, G. W.; Schlegel, H. B.; Scuseria, G. E.; Robb, M. A.; Cheeseman, J. R.; Scalmani, G.; Barone, V.; Petersson, G. A.; Nakatsuji, H. *et al.* Gaussian 16, Revision A.03, Gaussian, Inc., Wallingford CT, 2016.
- (35) Hariharan, P.C.; Pople, J.A. The influence of polarization functions on molecular orbital hydrogenation energies. *Theor. Chim. Acta* **1973**, *28*, 213-222.
- (36) Grimme, S.; Antony, J.; Ehrlich, S.; Krieg, H. A. consistent and accurate ab initio parametrization of density functional dispersion correction (DFT-D) for the 94 elements H-Pu. *J. Chem. Phys.* **2010**, *132*, 154104.
- (37) Grimme S, Ehrlich S, Goerigk L. Effect of the damping function in dispersion corrected density functional theory. *J. Comput. Chem.* **2011**, *32*, 1456-1465.
- (38) Byun, Y.-M.; Ullrich, C.A.; Excitons in Solids from Time-Dependent Density-Functional Theory: Assessing the Tamm-Dancoff Approximation. *Computation* **2017**, *5*, 9.
- (39) Dreuw, A.; Head-Gordon, M. Single-reference ab initio methods for the calculation of excited states of large molecules. *Chem. Rev.* **2005**, *105*, 4009-4037.
- (40) Casida, M.E; Huix-Rotllant, M. Progress in time-dependent density-functional theory. *Annu. Rev. Phys. Chem.* **2012**, *63*, 287–323.
- (41) Casida, M.E. Charge-transfer correction for improved time-dependent local density approximation excited-state potential energy curves: Analysis within the two-level model with illustration for H<sub>2</sub> and LiH. *J. Chem. Phys.* **2000**, *113*, 7062.

(42) Chantzis, A.; Laurent, A.D.; Adamo, C.; Jacquemin, D. Is the Tamm-Dancoff Approximation reliable for the calculation of absorption and fluorescence band shapes? *J. Chem. Theory Comput.* **2013**, *9*, 4517-4525.

(43) Isegawa, M.; Truhlar, D.G. Valence excitation energies of alkenes, carbonyl compounds, and azabenzenes by time-dependent density functional theory: Linear response of the ground state compared to collinear and noncollinear spin-flip TDDFT with the Tamm-Dancoff approximation. *J. Chem. Phys.* **2013**, *138*, 134111

(44) Hu, C.; Sugino, O.; Watanabe, K. Performance of Tamm-Dancoff approximation on nonadiabatic couplings by time-dependent density functional theory. *J. Chem. Phys.* **2014**, *140*, 054106.

(45) Hanwell, M.D.; Curtis, D.E.; Lonie, D.C.; Vandermeersch, T.; Zurek, E.; Hutchison, G.R. Avogadro: an advanced semantic chemical editor, visualization, and analysis platform. *J. Cheminf.* **2012**, *4*, 17.

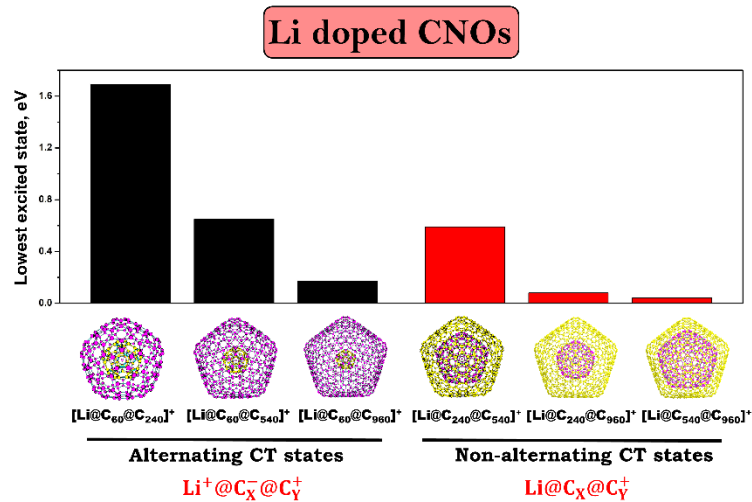
(46) Avogadro: an open-source molecular builder and visualization tool. Version 1.20. <http://avogadro.cc/>

(47) Grimme, S. A simplified Tamm-Dancoff density functional approach for the electronic excitation spectra of very large molecules. *J. Chem. Phys.* **2013**, *138*, 244104.

(48) Goerigk, L; Grimme, S. Assessment of TD-DFT methods and of various spin scaled CIS(D) and CC2 versions for the treatment of low-lying valence excitations of large organic dyes. *J. Chem. Phys.* **2010**, *132*, 184103.

- (49) Risthaus, T.; Hansen, A.; Grimme, S. Excited states using the simplified Tamm-Dancoff-Approach for range-separated hybrid density functionals: development and application. *Phys. Chem. Chem. Phys.* **2014**, *6*, 14408-14419.
- (50) Plasser, F.; Lischka, H. Analysis of Excitonic and Charge Transfer Interactions from Quantum Chemical Calculations. *J. Chem. Theory Comput.* **2012**, *8*, 2777-2789.
- (51) Plasser, F.; B  ppler, S.A.; Wormit, M.; Dreuw, A. New tools for the systematic analysis and visualization of electronic excitations. II. Applications. *J. Chem. Phys.* **2014**, *141*, 024107.
- (52) Newton, M. D. Quantum chemical probes of electron-transfer kinetics: the nature of donor-acceptor interactions. *Chem. Rev.* **1991**, *91*, 767–792.

## Table of Contents/ Abstract Graphic



The lowest-lying charge transfer state in carbon nano-onions doped with Li<sup>+</sup> depends strongly on the size of the concentric fullerenes and may be tuned by varying the outer or inner shells.